Int. J. Electrochem. Sci., 12 **(2017)** 9812 – 9828, doi: 10.20964/2017.10.81

International Journal of ELECTROCHEMICAL SCIENCE
www.electrochemsci.org

Application of Newly Quiniline-3-carbonitriles as Corrosion Inhibitors on Mild Steel in 1.0 M HCl: Electrochemical Measurements, HF and DFT/B3LYP Calculations

Nuha Wazzan[1,*] *and Saedah Al-mhyawi*[1]

[1]King Abdulaziz University, Chemistry Department, Faculty of Science, P.O Box 42805 Jeddah 21589, Saudi Arabia
[*]E-Mail: nwazzan@kau.edu.sa

Received: 12 May 2017 / *Accepted:* 17 August 2017 / *Published:* 12 September 2017

In combined experimental and theoretical studies, two new derivatives of quinolone-3-carbonitrile were tested for their anti-corrosive properties for mild steel in a 1.0 M HCl medium. The studied compounds were 4-(4-nitrophenyl)-2-oxo-1,2,5,6-tetrahydrobenzo[*h*]quinoline-3-carbonitrile (NPQC) and 4-(furan-3-yl)-2-oxo-1,2,5,6-tetrahydrobenzo[*h*]quinoline-3-carbonitrile (FQC). The inhibition efficiencies were investigated using electrochemical techniques at different inhibitor's concentrations and temperatures. This study revealed that NPQC and FQC are good inhibitors, and the inhibition efficiency order was NPQC > FQC. The correlation between their molecular reactivity and inhibition efficiency was investigated by two methods (HF and DFT/B3LYP) with two basis sets (6-31+G(d) and 6-311++G(d,p)) in the gas phase and aqueous solution, applying the conductor polarizable continuum model of solvation. The quantum chemical parameters of the neutral and all possible protonated forms of the two inhibitors were evaluated. Very good correlations between the experimental and theoretical data were obtained. Modeling the inhibitor-Fe complexes of the neutral and protonated forms of the inhibitors predicts that N16 is the active site for the adsorption process for both inhibitors. The calculations of the energies of inhibitor-Fe complexes and the N16-Fe bond lengths justify the superior inhibition efficiency of NPQC compared to that of FQC.

Keywords: Anti-corrosive; mild steel; Quinoline-3-carbonitriles; DFT/B3LYP calculations; Quantum chemical parameters.

1. INTRODUCTION

Metal corrosion is a major industrial problem that has led a large amount of research and investigations [1, 2]. The efficiency of inhibitors depends on the nature of the metal surface, number of adsorption active centers in the inhibitor and molecular size [3].The organic compounds of

heterocyclic (cyclic aromatic or non-aromatic) with N, S, and or O atoms are widely used as effective corrosion inhibitors for several industrial metals in corrosive media. Additionally, functional electronegative groups and π-electrons in triple or conjugated double bonds enable inhibitors to adsorb to the metal surface and form protective complex layers [4]. The advantages of the organic (metal free) inhibitors rose from their low-cost, easy-preparation and purification steps, and environmentally-friendly nature (large number proved as potential bioactive compounds). Quinoline-3-carbonitrile derivatives are nitrogen containing heterocyclic aromatic compounds. Most of these derivatives are known to be non-toxic compounds with large pharmacological and biological activities. Some are reported as anticancer [5], antibacterial [6], and they have been reported as active drugs in the treatment of Alzheimer's disease [7] and rheumatoid arthritis [8]. Lately, researchers synthesized and used quinoline-3-carbonitrile derivatives as corrosion inhibitors. [8, 9]

Two synthetic pathways were adopted to synthesize new derivatives of organic quinoline-3-carbonitrile [10]. The structure of the synthesized compounds has been confirmed by elemental analyses, ^{1}H and ^{13}C NMR, and FT-IR. On the other hand, iron metal is considered as a spinal column of the new industry, minimization of its corrosion attracts many attentions especially in corrosive acidic media [9, 11].

The quantum chemical calculations have been widely used to relate between the inhibition efficiency of the inhibitors and their molecular properties [12, 13]. Nowadays, density functional theory (DFT) becomes one of the most promising tools, because of its low-cost, accurate and effective results. From which many important parameters called the quantum chemical parameters (QCPs) could be obtained for even large and complex molecular systems in very reasonable time.

In this study, the anti-corrosive properties of two of those new synthesized derivatives for iron metal (mild steel) in a corrosive medium (1.0 M HCl) were performed. The two investigated compounds were 4-(4-nitrophenyl)-2-oxo-1,2,5,6-tetrahydrobenzo[*h*]quinoline-3-carbonitrile and 4-(furan-3-yl)-2-oxo-1,2,5,6-tetrahydrobenzo[*h*]quinoline-3-carbonitrile, abbreviated as NPQC and FQC, respectively [10]. The corrosion behavior was tested using the experimental electrochemical techniques including the electrochemical impedance spectroscopy and potentiodynamic polarization in the absence and presence of different concentrations of inhibitors at different temperatures (303, 313, 323 and 333 K). The experimental findings revealed that:

a) The two compounds showed efficient inhibition and the inhibition efficiency of the NPQC is superior to that of FQC,

b) The inhibition efficiency increases with an increase in the concentration of inhibitor and decreases with an increase in temperature,

c) The spontaneity of the adsorption process was revealed from the thermodynamic parameters, and

d) The strong adsorption and the physical adsorption mechanism were evident from the negative values of $\Delta G°$.

The details and results of the experimental study are provided in the supplementary data.

To achieve deep understanding of the inhibition properties at the molecular level, the experimental finding was combined by quantum chemical calculations. In this study, HF and DFT/B3LYP calculations were used to interpret the relationship between the geometrical structures

and the inhibition abilities. The molecular structures of the investigated compounds are depicted in Scheme 1.

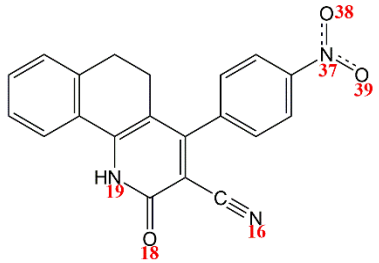

4-(4-nitrophenyl)-2-oxo-1,2,5,6-tetrahydrobenzo[*h*]quinoline-3-carbonitrile (NPQC)

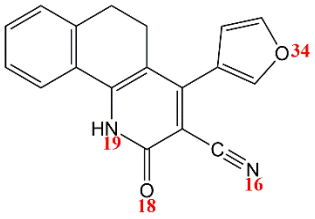

4-(furan-3-yl)-2-oxo-1,2,5,6-tetrahydrobenzo[*h*]quinoline-3-carbonitrile (FQC)

Scheme 1. Chemical structures of NPQC and FQC along with the atomic numbering of the heteroatoms, their IUPAC names, and abbreviations used throughout the present study.

2. DFT DETAILS

The Gaussian 09 suite program was used to perform the calculations [14]. Geometry optimizations were conducted by DFT using Becke's three parameter exchange functional [15], and the Lee–Yang–Parr correlation functional (B3LYP) [16] and Hartree-Fock (HF) [17]. These methods were applied with 6-31G(d) and 6-311++G(d,p) basis sets. In the geometry optimizations of the neutral and protonated forms of the inhibitors, each bond length, bond angle and the dihedral angle were optimized without any constraints. The nature of the stationary points was confirmed by vibrational frequency analysis to verify that no imaginary frequencies (negative frequencies) were obtained. Since the experimental data were executed in acidic aqueous solution; the calculations accounted for solvent effect by applying the well-tested self-consistent reaction field (SCRF) theory, with the conductor polarizable continuum model (CPCM) of solvation [18]. Visual inspections were performed using the GaussView program (version 5.0.8) [19] and Chemcraft program version 1.8 (build 489) [20].

3. RESULTS AND DISCUSSION

3.1 Neutral forms of inhibitors

The quantum chemical parameters (QCPs) for the neutral (non-protonated) forms of the investigated inhibitors calculated by the above mentioning methods (HF and DFT/B3LYP) with the 6-31+G(d) and 6-311++G(d,p) in the gas phase and aqueous solution are listed in Table 1and Table 2. Analysis of the data will be given in the following paragraphs.

Frontier molecular orbital (FMO) analysis: The frontier molecular orbital are the highest occupied molecular orbital (HOMO) and the lowest unoccupied molecular orbital (LUMO) and their influential role in chemical reactivity has been demonstrated by Fukui [21]. The electron-releasing

ability of a molecule is expressed by the HOMO energy. Larger values (destabilized) of E_{HOMO} indicate a real ability of the molecule to donate electrons from the π rich-electron heteroaromatic system to the *d*-orbital of iron atoms on the steel surface that is partially empty. On the other hand, the electron withdrawing ability of a molecule is expressed by the LUMO energy. Lower values (stabilized) of E_{LUMO} indicate a good ability to withdraw electrons from the *d*-orbital of the iron atoms that is partially filled. Thus, the adsorption process between the inhibitor molecules and the metal (iron in this study) surface proceeds in two directions: electron donation from the HOMO level of the inhibitor to the partially empty *d*-orbital of iron atoms and electron-back-donation from the partially filled *d*-orbital of iron atoms to the LUMO level of the inhibitor. Inspection of Table 1 and Table 2 reveals that E_{HOMO} increases (less stabilized) from NPQC to FQC, which means that the electron-releasing ability of NPQC is weaker than that of FQC. E_{LUMO} of NPQC decreases (more stabilized) than that of FQC, which indicates that the electron-withdrawing ability of NPQC from the steel surface is better than that of FQC. On the other hand, the HOMO-LUMO energy gap (HLG) is a parameter that measures the chemical reactivity; a small HLG reflects a reactive molecule and *vice versa*. Good inhibitor efficiency will be combined by lower HLG because lower HLG facilitates the electron removal from the LUMO level of the inhibitor in the electron-back-donation process to the metal surface.[22, 23] As an example, the HLG value of NPQC is smaller than that of FQC by ~0.2 eV at B3LYP/6-311++G(d,p) in the gas phase. Thus, FMO analysis provides us with an explanation for the experimental results that show that NPQC has a better ability to inhibit the corrosion of iron. NPQC, which has a lower LUMO energy and smaller energy gap compared to those of FQC, showed better charge transfer during the adsorption process of the inhibitor on the steel surface. The HOMO energies of the two inhibitors could not explain their inhibition performances.

Table 1. Calculated QCPs (in eV) for the neutral forms of the investigated inhibitors in the gas phase.

	E_{HOMO}	E_{LUMO}	*IE*	*EA*	HLG	η	σ	χ	ω/D^2.eV^{-1}	μ(/D)	ΔE_{tot}	$\Delta N/e$
HF/6-31+G(d)												
NPQC	-8.64	0.58	8.64	-0.58	9.22	4.61	0.22	4.03	70.57	11.96	-1.15	0.32
FQC	-8.39	0.91	8.39	-0.91	9.30	4.65	0.22	3.74	62.20	10.63	-1.16	0.35
B3LYP/6-31+G(d)												
NPQC	-6.54	-3.18	6.54	3.18	3.36	1.68	0.59	4.86	189.90	11.74	-0.42	0.64
FQC	-6.27	-2.66	6.27	2.66	3.60	1.80	0.56	4.46	155.76	10.31	-0.45	0.70
HF/6-311++G(d,p)												
NPQC	-8.65	0.59	8.65	-0.59	9.24	4.62	0.22	4.03	69.80	11.85	-1.16	0.32
FQC	-8.40	0.72	8.40	-0.72	9.12	4.56	0.22	3.84	62.64	10.50	-1.14	0.35
B3LYP/6-311++G(d,p)												
NPQC	-6.58	-3.16	6.58	3.16	3.42	1.71	0.58	4.87	184.67	11.61	-0.43	0.62
FQC	-6.31	-2.70	6.58	2.70	3.61	1.81	0.55	4.51	153.44	10.19	-0.45	0.69

Table 2. Calculated QCPs (in eV) for the neutral forms of the investigated inhibitors in the aqueous solution.

	E_{HOMO}	E_{LUMO}	*IE*	*EA*	HLG	η	σ	χ	ω/D^2.eV^{-1}	μ(/D)	ΔE_{tot}	$\Delta N/e$
HF/6-31+G(d)												
NPQC	-8.39	0.79	8.39	-0.79	9.18	4.59	0.22	3.80	94.71	15.97	-1.15	0.348
FQC	-8.35	0.94	8.35	-0.94	9.29	4.64	0.22	3.70	84.71	14.46	-1.16	0.355
B3LYP/6-31+G(d)												
NPQC	-6.36	-3.24	6.36	3.24	3.12	1.56	0.64	4.80	284.57	16.31	-0.39	0.71
FQC	-6.29	-2.63	6.29	2.63	3.66	1.83	0.55	4.46	217.03	14.61	-0.46	0.69
HF/6-311++G(d,p)												
NPQC	-8.40	0.81	8.40	-0.81	9.21	4.60	0.22	3.79	93.55	15.83	-1.15	0.348
FQC	-8.36	0.94	8.36	-0.94	9.30	4.65	0.22	3.71	83.74	14.30	-1.16	0.354
B3LYP/6-311++G(d,p)												
NPQC	-6.40	-3.23	6.40	3.23	3.17	1.59	0.63	4.81	275.86	16.07	-0.40	0.690
FQC	-6.34	-2.67	6.34	2.67	3.67	1.83	0.55	4.50	213.99	14.42	-0.46	0.681

Dipole moment: Some literature reports show a direct relationship between the dipole moments and inhibition efficiencies [24, 25], and other reports show an inverse relationship [26, 27]. As suggested [28], physisorption of the inhibitor on the metal surface results from an electrostatic interaction between charged sites in the inhibitor and metal and, in turn, results in a dipole-dipole interaction. Thus, the direct relationship between the dipole moments of the inhibitors and their inhibition efficiencies suggests physical adsorption. The dipole moments of the neutral forms of NPQC and FQC have a direct relationship with their inhibition efficiencies (in the gas phase and aqueous solution); this predicts that the two inhibitors are physically adsorbed on the iron surface, as revealed experimentally.

Global hardness and softness: According to Janak's theorem and to the valence state parabola model, global hardness (/absolute hardness, the value in some environment is different from that for isolated molecule) can be represented regarding HOMO's and LUMO's energies: [22, 29-31]

$$\eta = -\frac{E_{LUMO} - E_{HOMO}}{2} = \frac{IE - EA}{2} \quad \textbf{(1)}$$

The inverse of the global hardness gives the global softness:

$$\sigma = \frac{1}{\eta} \quad \textbf{(2)}$$

According to the hard-soft-acid-base theory (HSABT) and because the metal atoms are considered to be soft acids, the inhibitor with the lower hardness and larger softness values (the softer inhibitor) will interact with and adsorb on the metal surface more readily than the harder inhibitor. In Table 1 and Table 2, the neutral forms of NPQC (in gas and aqueous solution) have a lower η and larger σ values; thus, it is softer than FQC, which explains the higher inhibition efficiency of NPQC. Additionally, NPQC, which has a small HLG and low hardness, is more reactive toward the iron surface. This is consistent with the Maximum Hardness Principal, which states that the molecules in nature are arranging themselves as hard as possible [32].

Global electronegativity: The global electronegativity (χ)is given by: [29, 33]

$$\chi = \frac{IE + EA}{2} \quad \textbf{(3)}$$

It has been reported that better inhibition efficiencies are correlated with lower electronegativities [25, 34]. This is attributed to the fact that an inhibitor with a low χ value is better able to give electrons to the metal. Comparing the χ values of the two inhibitors under investigation shows that NPQC has a larger value than that of FQC, a result that is not consistent with the experimental inhibition efficiencies.

Global electrophilicity: The global electrophilicity index (ω) is a parameter that indicates the ability of the inhibitor to withdraw electrons. [35] The global electrophilicity index is given by:

$$\omega = \frac{\mu^2}{2\eta} \quad \textbf{(4)}$$

The ω values of neutral forms of NPQC are greater than that of FQC at all methods and basis sets in the gas phase and aqueous solution. As an example, the ω value of NPQC is 31 $D^2.eV^{-1}$ greater than that of FQC at B3LYP/6-311++G(d,p) in the gas phase. Thus, NPQC exhibits a higher ω value, which confirms its superior ability to withdraw electrons. A coordinate bond is formed when the unoccupied *d*-orbitals of the Fe atom receive electrons from the inhibitor molecule. A back-donating bond is formed when the inhibitor molecule receives electrons from the Fe atom. These donation and back-donation processes reinforce the adsorption of NPQC onto the iron surface [36]; the theoretically values observed agreed with the experimental observations.

The fraction of electrons transferred: The fraction of electrons transferred from the inhibitor to the metal surface is denoted as ΔN , according to Pearson it is given by: [33]

$$\Delta N = \frac{\chi_{\mathrm{Fe}} - \chi_{\mathrm{inh}}}{2(\eta_{\mathrm{Fe}} + \eta_{\mathrm{inh}})} \quad \textbf{(5)}$$

Where χ_{Fe} and χ_{inh} are the global electronegativity of the iron metal and inhibitor, respectively, and η_{Fe} and η_{inh} are the global hardness of the iron metal and inhibitor, respectively. The common theoretical values of global electronegativity and hardness for iron in the bulk metal (7.0 eV/mol and 0.00 eV/mol, respectively) were used [37].

When $\Delta N > 0$, electron transfer from the inhibitor to the iron is high and when $N < 0$, electron transfers from the inhibitor to the iron is low. ΔN values show that the inhibition effect resulting from the donation of electrons. The inhibition efficiency increases with the increasing electron-releasing ability at the metal surface when $\Delta N < 3.6$ [38]. The ΔN values of NPQC and FQC are much smaller than 3.6. Thus, the two inhibitors act as electrons donors, and the iron surface serves as the acceptor, thus binding the inhibitor to the iron surface and resulting in a layer of adsorption between the inhibitor and metal that protects from corrosion. It was reported that increasing inhibition efficiencies corresponded with increasing ΔN values. However, the neutral form of NPQC at most method/basis set, which has higher inhibition efficiency, has a lower ΔN value. It is worth mentioning that ΔN is preferably called the electron-donating ability rather than the number of electrons transferred since it does not refer to the exact number of electrons transferred from the inhibitor as donor molecule to the iron as acceptor atom [22].

Total energy change: The total energy change denoted as ΔE_{tot} is the energy change associated with two process occurring in the inhibitor molecule: [39] (1) receiving of electrons at some center, and (2) the back-donation of electrons from the same center or from other active centers. Similar to the results found in the literature, [40] $\eta > 0$ and $\Delta E_{tot} < 0$, Table 1and Table 2, implying that it is energetically favorable for the charge to transfer to a molecule (NPQC and FQC) then by back-donation from the molecule. The calculated ΔE_{tot} value for NPQC is larger (less negative) than that of FQC, suggesting that the inhibition efficiency of NPQC is better than that of FQC, as shown experimentally.

Molecular electrostatic maps: NPCQ and FQC have three possible sites (N16, N19, and O18 atoms) for electrophilic attack. At B3LYP/6-311++G(d,p) in the gas phase as a representative example, the three fused rings are relatively negative regions. Additionally, the nitrophenyl and furan rings have relatively negative regions. For NPQC, there are three other possible sites for electrophilic attack (N37, O38, and O39), and FQC has another potential site for electrophilic attack (O34). From the calculated regions of the molecular electrostatic maps (MEPs) of NPQC and FQC (Figure 1), the negative regions are delocalized on the electronegative atoms (oxygen and nitrogen) in addition to the fused and substituted rings. The positive regions are delocalized on the hydrogen atoms. Thus, the interaction between the inhibitor molecules and the mild steel surface leads to electron transfer. This result means that the electronegative atoms (heteroatoms) are the active atoms in the studied inhibitors. Moreover, iron acts as an electrophilic center that can attract the negatively charged sites of the inhibitor molecule.

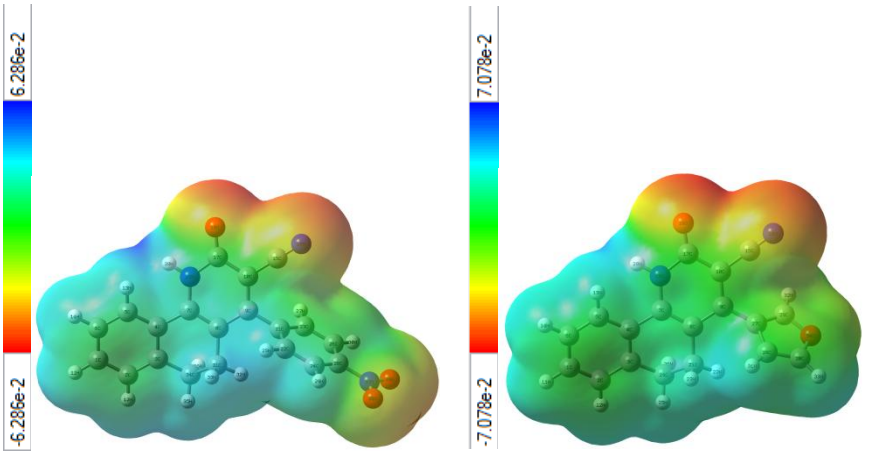

	Partial charge	
	NPQC	FQC
N16	-0.038	-0.043
O18	-0.027	-0.037
N19	0.016	0.0007
N37	-0.020	–
O38	-0.026	–
O39	-0.026	–
O34	–	-0.008

Figure 1. Molecular electrostatic map of the investigated inhibitors at B3LYP/6-311++G(d,p) in the gas phase.

Examining the partial charges of the heteroatoms of the two inhibitors reveals that, as expected, most of these atoms are negatively charged, except the N19 atoms, which have with minimal positive charges (Figure 1). This is because the lone pairs of electrons of N19 are involved in the conjugation of the ring.

Figure 2 shows the FMOs (HOMO and LUMO orbitals) of the inhibitors. From this figure, we can see that the two inhibitors are rich in electrons and simultaneously able to donate electrons to the

iron surface, this leads to better anti-corrosive properties for the inhibitor because of the enhancement formation of inhibitor layer. Furthermore, the LUMO orbitals show the electron withdrawing parts of the inhibitors during the interaction with a metal surface. The HOMO distribution on the two inhibitors is relatively similar; it is delocalized over most of the molecule, except for the nitrophenyl and furan rings of NPQC and FQC, respectively. However, the LUMO distribution in FQC is relatively similar to its HOMO distribution. By contrast, in NPQC, LUMO is distributed over almost the entire molecule, including the nitrophenyl ring. The electron-donating portions of the two molecules with respect to the iron surface are relatively similar, while the electron-back-donation from iron to the inhibitors is greater in NPQC than in FQC; this explains the higher inhibition efficiency of NPQC compared to that of FQC.

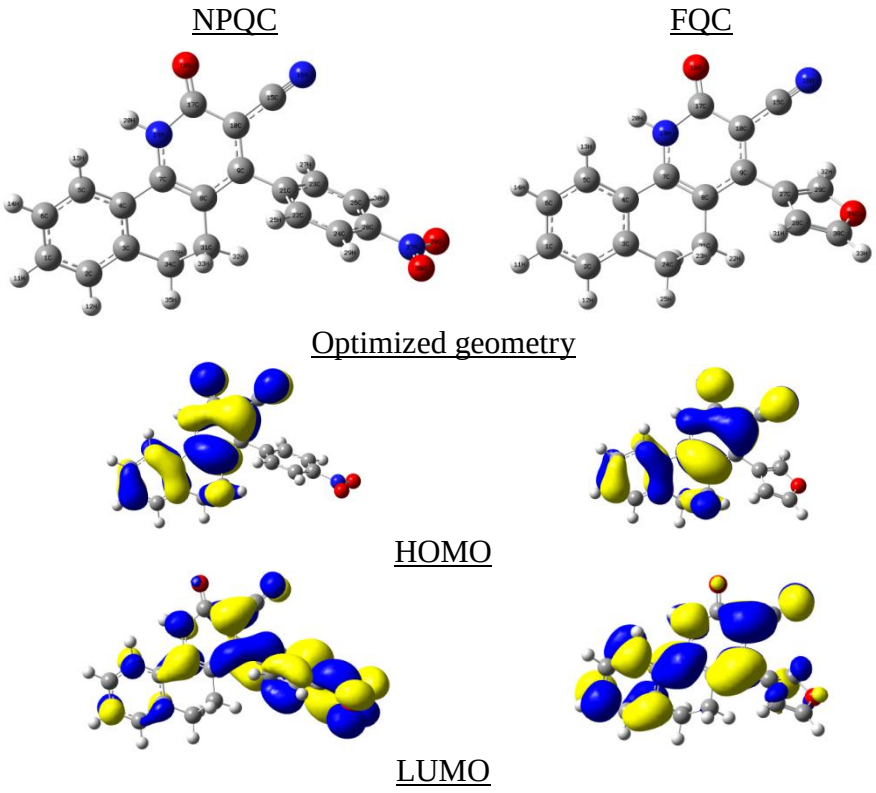

Figure 2. Optimized geometries and FMO distributions of the neutral forms of the investigated inhibitors at B3LYP/6-311++G(d,p) in the gas phase.

Coefficients of HOMO and LUMO orbitals: To gain better insight into the distribution of HOMO and LUMO orbitals, the coefficients of these orbitals were calculated at B3LYP/6-311++G(d,p) in the gas phase, Table 3. These coefficients give information about the atomic orbital with the highest contribution to the formation of FMOs and thus the atom that has the highest tendency to donate electrons (from the HOMO) or accept electrons (to the LUMO) [34]. In support of the information from the MEP and FMO plots, Figure 1 and Figure 2, respectively, the common heteroatoms between the two inhibitors have the highest coefficients of the HOMO. This indicates that these atoms, in particular, have the highest ability to give electrons to the iron surface. However, the highest coefficients of the LUMO are from N16 and N19 in FQC, but only from N19 in NPQC. The

O18 atom in the two inhibitors, according to the coefficients of the HOMO and LUMO orbitals, has the ability to give electrons but to not receive electrons from the *d*-orbital of Fe atoms during the back-donation process. Back-donation in NPQC is covered by the other heteroatoms, *i.e.*, N37, O38 and O39 atoms, as shown from their highest coefficient values to the LUMO orbital. The contributions of the O34 atom in FQC to the HOMO and LUMO orbitals are relatively small. However, other atoms in the two molecules appeared to significantly contribute both/either to HOMO and LUMO. The C3 atom has the highest coefficients to both LUMO and HOMO for the two molecules. The C17 atom has the highest contribution to LUMO in NPQC and a small coefficient to that orbital in FQC. In conclusion, NPQC has contributions from N16, O18, N19, N37, O38, O39, C3 and C17, with large coefficients to HOMO and LUMO.

Table 3. The highest coefficients of the HOMO and LUMO of the neutral forms of the investigated inhibitors

	Atomic numbering									
	C3	C17	C24	N16	N19	O18	N37	O38	O39	O34
	Maximum coefficient of the HOMO									
NPQC	0.392	0.059	0.094	0.124	-0.133	0.183	-0.012	0.004	0.005	−
FQC	0.316	0.050	0.293	-0.125	0.134	-0.189	−	−	−	-0.013
	Maximum coefficient of the LUMO									
NPQC	-0.241	0.176	0.236	0.075	0.114	0.025	0.227	-0.179	-0.178	−
FQC	0.610	0.034	0.857	-0.130	-0.196	-0.028	−	−	−	-0.030

See Figure 2 for atomic numbering

By contrast, FQC has contributions from a lower number of atoms, *i.e.*, N16, O18, N19, and C3. This means that the processes of electron donation and electron-back-donation between the inhibitor and the metal surface are more predominant in NPQC than in FQC. This enforces the adsorption of NPQC on the iron surface and may explain its better inhibition efficiency compared to that of FQC.

3.2 Protonated forms of inhibitors

In an acidic medium (1 M HCl) and because of the presence of heteroatoms with lone pairs of electrons, NPQC and FQC most likely act as bases and attract protons. For this reason, all of the possible sites for the protonation process, *i.e.*, the N16, O18, N19, N37, O38, O39 and O34 atoms, of the two investigated inhibitors were calculated (Table 4 and

Table 5). The degree of protonation was measured by calculating the proton affinity (*PA*) at each possible protonated site for both inhibitors using equation 6: [40]

$$PA = E_{\text{prot}} + E_{\text{H}_2\text{O}} - E_{\text{nuetral}} - E_{\text{H}_3\text{O}^+} \quad \textbf{(6)}$$

where $E_{\text{prot}}, E_{\text{H}_2O}, E_{\text{nuetral}}$ and $E_{\text{H}_3\text{O}^+}$ are the sum of electronic and thermal enthalpies of the protonated, water, neutral and a hydronium ion, respectively.

The stability data for the neutral and protonated forms of NPQC and FQC at B3LYP/6-311++G(d,p) level of theory in the gas phase and aqueous solution are summarized in Table 4 and Table 5, respectively. Table 4 and Table 5 show that, for both inhibitors, the most probable site for the protonation process is the O18 atom. This result is in total agreement with the findings from the MEP maps. From these maps, the O18 atom showed the potential only to donate electrons.

Table 4. Relative energies (/kcal mol^{-1}), the sum of the electronic and thermal enthalpies (/a.u.) and proton affinities (/kcal mol^{-1}) for neutral and all of the possible protonated forms of the NPQC and FQC inhibitors at the B3LYP/6-311++G(d,p) in the gas phase. Data in bold font represent the most stable protonated forms

Inhibitor designation	Protonated form	*RE*	$E_{elec} + H$	*PA*
NPQC	Neutral	225.71	-1159.798	–
	PN16	9.01	-1160.132	-46.68
	PN19	41.94	-1160.078	-13.17
	PN37	–	–	–
	PO18	**0.00**	**-1160.144**	**-54.65**
	PO38	22.69	-1160.109	-32.63
	PO39	22.56	-1160.110	-32.74
FQC	Neutral	224.26	-953.050	–
	PN16	2.43	-953.392	-51.79
	PN19	33.14	-953.342	-20.32
	PO18	**0.00**	**-953.395**	**-53.39**
	PO34	50.72	-953.316	-3.65

Table 5. Relative energies (/kcal mol^{-1}), the sum of the electronic and thermal enthalpies (/a.u.) and proton affinities (/kcal mol^{-1}) for neutral and all of the possible protonated forms of the NPQC and FQC inhibitors at the B3LYP/6-311++G(d,p) in the aqueous solution. Data in bold font represent the most stable protonated forms.

Inhibitor designation	Protonated form	*RE*	$E_{elec} + H$	*PA*
NPQC	Neutral	262.24	-1159.83	–
	PN16	11.76	-1160.21	-98.51
	PN19	33.09	-1160.18	-75.98
	PN37	–	–	–
	PO18	**0.00**	**-1160.23**	**-109.02**
	PO38	19.34	-1160.20	-90.14
	PO39	19.29	-1160.20	-90.11
FQC	Neutral	262.13	-953.07	–
	PN16	10.24	-953.46	-96.83
	PN19	30.50	-953.43	-75.51
	PO18	**0.00**	**-953.48**	**-105.74**
	PO34	37.80	-953.42	-68.91

By contrast, the other sites showed the potential to donate and accept electrons at the same time or showed no tendency to donate electrons. *PA* decreases in the following order: O18 > N16 > O39 > O38 > N19 and O18 > N16 > N19 > O34 for NPQC and FQC, respectively. The calculations prove that the protonated forms are more stable than their counterpart neutral forms by ~225 kcal/mol in the gas phase (Table 4) ; thus, both inhibitors have a significant ability for protonation. The N16 atom can be considered to be a competing site for protonation; the *PA* values at this site for both inhibitors are smaller than those at the O18 site by only ~2 kcal/mol. Thus, the protonation at this site cannot be ignored. In the aqueous solution, the stabilities of the protonated forms become even more important, Table 5.

It was reported that as the *PA* becomes more negative, the inhibitor becomes more basic. Consequently, NPQC has a more basic (and less acidic) character. NPQC shows higher *PA* values at all protonation sites. For instance, the *PA* at the most stable site (O18) of NPQC is more negative than that at the same site of FQC by ~1.2 kcal/mol. Additionally, it was reported that as basicity of organic compound increases, its inhibition efficiency increases. [34] This result is in total agreement with experiment that proved the superiority of NPQC as an inhibitor compared to FQC.

Table 6. Calculated QCPs for the most stable protonated forms of the investigated inhibitors at the B3LYP/6-311++G(d,p) in the gas phase, regular font and aqueous solution, bold font.

Inhibitor designation	E_{HOMO} (*IE*) /eV	E_{LUMO} (*EA*) /eV	HLG /eV	η /eV	χ /eV	ω / $D^2.eV^{-1}$	μ /D	ΔE_{tot} /eV	ΔN /e
NPQC (PO18)	-10.53 (10.53)	-6.88 (6.88)	3.65	1.82	8.70	201.50	13.51	-0.46	-0.47
	-7.26 (7.26)	**-3.55 (3.55)**	**3.71**	**1.86**	**5.41**	**256.19**	**17.49**	**-0.46**	**0.429**
NPQC (PN16)	-10.25 (10.25)	-7.01(7.01)	3.24	1.62	8.63	134.35	7.99	-0.40	-0.50
	-7.09 (7.09)	**-3.77 (3.77)**	**3.32**	**1.66**	**5.43**	**146.03**	**8.90**	**-0.41**	**0.473**
FQC (PO18)	-9.96 (9.96)	-6.58 (6.58)	3.38	1.69	8.27	116.23	7.22	-0.42	-0.37
	-7.05 (7.05)	**-3.37 (3.37)**	**3.69**	**1.84**	**5.21**	**148.98**	**10.10**	**-0.46**	**0.485**
FQC (PN16)	-9.93 (9.93)	-6.80 (6.80)	3.13	1.56	8.37	36.63	2.10	-0.39	-0.44
	-6.94 (6.94)	**-3.69 (3.69)**	**3.25**	**1.62**	**5.31**	**52.61**	**3.14**	**-0.41**	**0.519**

To correlate between the QCPs and inhibition efficiencies of the protonated forms of the investigated inhibitors, we only consider the protonation at O18 and N16 atoms as the potential protonated sites because of their stabilities and higher *PA* values. The QCPs for the most stable protonated forms (PO18 and PN16) of both inhibitors in the gas phase and aqueous solution were calculated, Table 6. Additionally, to remark on the change in the QCPs upon protonation, the QCPs of the neutral and most stable protonated forms of the investigated inhibitors are represented in Figure 3.

Protonation results in a remarkable change in most of the QCPs of the two inhibitors and, consequently, a notable change in their reactivity toward the steel surface. Upon protonation in the gas phase and aqueous solution, the HOMO energies of the protonated forms are lower those that of neutral species; the abilities of the protonated forms to donate electrons are weaker than those of the neutral forms. The LUMO energies of the protonated forms are lower than those of the neutral forms;

thus, the abilities of the protonated forms to withdraw electrons are stronger than those of the neutral forms, and the HLG values decrease upon protonation (Figure 3). Additionally, the electronegativities of the protonated species are significantly increased upon protonation by ~4 eV in the gas phase. Interestingly, in the gas phase, the effect of the protonation process on the ΔN values is dramatic; these values are positive for neutral species, and for the protonated species, they become negative. This was observed in the literature and was attributed to the back-donation of electrons from metal (Fe) atoms to protonated inhibitor species. The back-donation of electrons is more feasible in protonated species than that in neutral forms due to the lower values of E_{LUMO} (Figure 3) [34, 41].

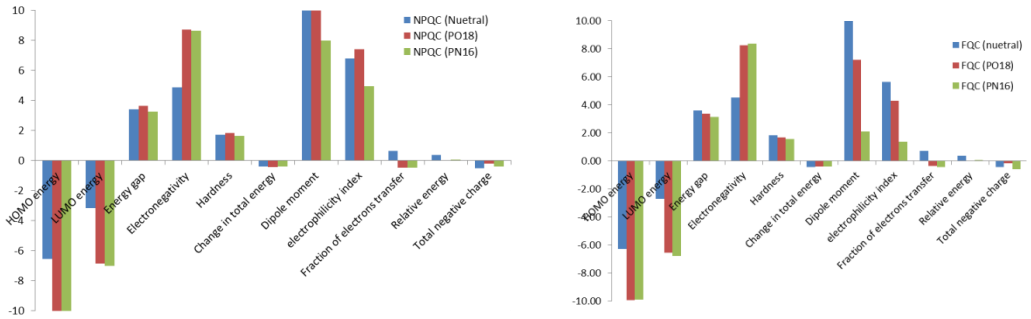

(a) (b)

Figure 3. QCPs of the neutral and most stable protonated forms of the investigated inhibitors (a) NPQC and (b) FQC.

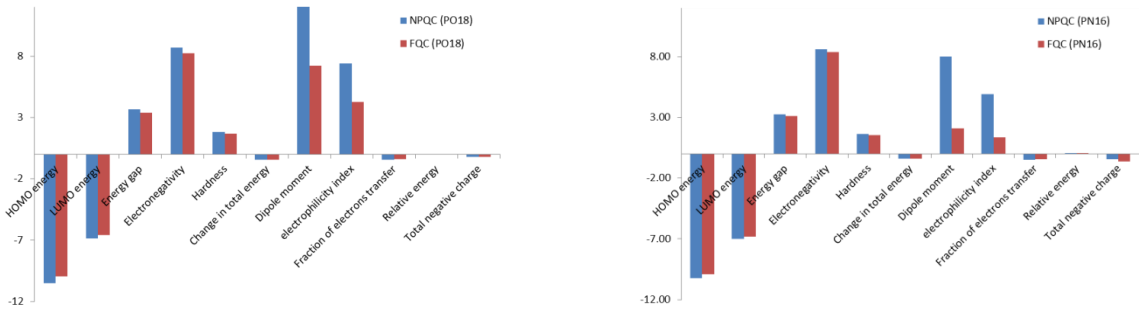

(a) (b)

Figure 4. QCPs of the most stable protonated forms of the investigated inhibitors (a) P(O18) and (b) P(N16).

The QCPs of the protonated species reveal that most of these parameters are not correlated very well with the experimentally determined inhibition efficiencies (Table 6 and Figure 4). Few parameters showed this correlation, *i.e.*, the energies of the LUMO, dipole moments and electrophilicity indexes. The trend of these parameters is NPQC > FQC, reflecting the better inhibition efficiency of NPQC compared to FQC. On the other hand, larger numbers of QCPs of the neutral forms are correlated more clearly with the tested inhibition efficiencies than those of the protonated forms [13, 34]. As reported in the literature, there are no complete correlations between the calculated QCPs and observed inhibition efficiencies in either the neutral or protonated forms. The adsorption of the inhibitor on the metallic surface is a complex process, and QCPs cannot fully describe this process, but it is also

evidence for the combined physisorption and chemisorption nature of the adsorption of these quinoline-3-carbonitrile derivatives [13, 34].

Figure 5 represents the LUMO and HOMO orbital distributions of the most stable protonated forms of the investigated inhibitors. Disagreeing with the trend showed for the QCPs, the protonation process did not markedly affect the distribution of these orbitals compared to those of the neutral form of the NPQC inhibitor (Figure 2). However, the HOMO distribution of protonated FQC, i.e., FQC (PN16) and FQC (PO18), is relatively different from that of neutral FQC. HOMO is mainly distributed on the substituted furane ring, more obviously so for FQC (PO18).

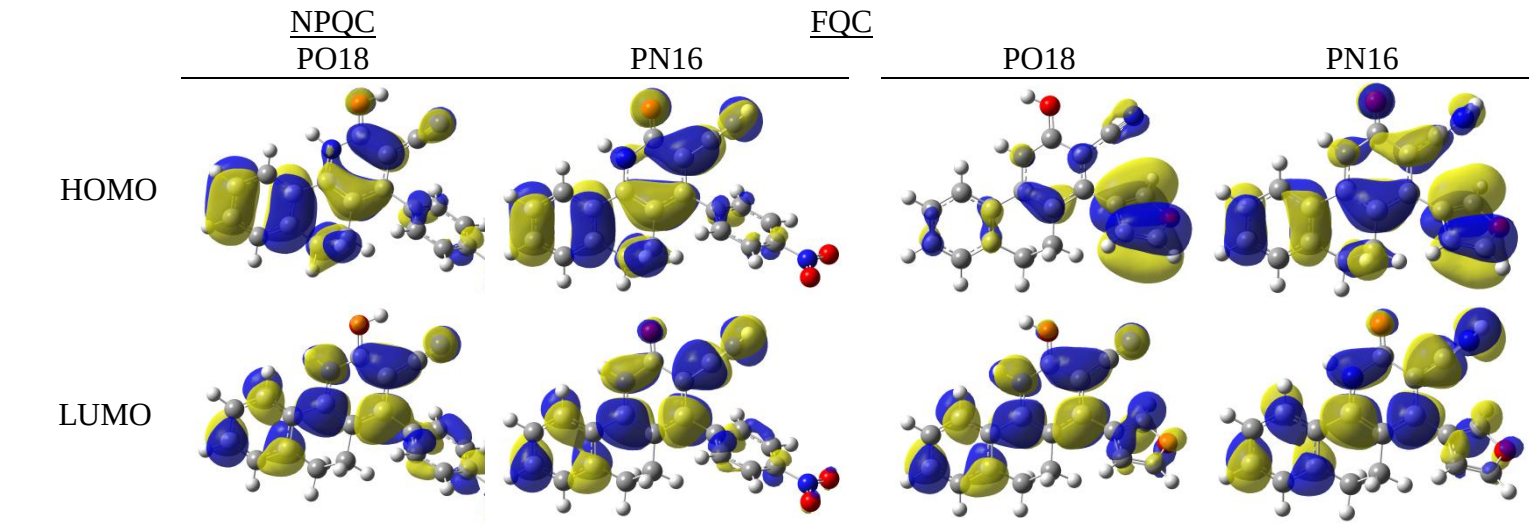

Figure 5. FMO distributions of the most stable protonated forms of the investigated inhibitors.

3.3 Mulliken population analysis for the neutral and protonated forms

Mulliken population analysis has been used extensively to predict the adsorption sites of inhibitor. The negatively charged heteroatom will be preferably adsorbed onto the iron surface by donor-acceptor interaction. At B3LYP/6-311++G(d,p) Mulliken population analysis was applied in both the neutral and protonated forms of NPQC and FQC, to determine where their anti-corrosive properties for mild steel in an acidic environment is due to their neutral or protonated forms.

Figure 6 shows the Mulliken charges population for the neutral and protonated forms (@O18) of NPQC and FQC at the B3LYP/6-311++G(d,p) in the gas phase. From

Figure 6, it is clear that the neutral forms of both inhibitors have higher negative charges on their heteroatoms. Thus, the protonation process decreases the strength of adsorption of the inhibitor through its active adsorption site (s) on the iron surface. It is reasonable here to sate that while O18 was proved as the preferred protonated site, another heteroatom(s) will be the preferred site(s) for the adsorption process. Investigation of the preferred site(s) for the adsorption process on the iron surface will be discussed in the next section.

For the neutral species in the gas phase and aqueous solution, the total negative charge (TNC) calculated from the partial Mulliken atomic charges on the heteroatoms (N and O) provides

information on the active centers that interact with the iron surface. As the atom becomes more negatively charged, the tendency to donate electrons increases [22, 34]. The common heteroatoms (N16, N19, and O18), of the two inhibitors, are all negatively charged, indicating that the two inhibitors will be adsorbed on the iron surface among these atoms. Comparing the TNC of common heteroatoms of NPQC and FQC could explain the better performance of NPQC as an inhibitor. For instance, the TNC for the neutral forms in the gas phase are -0.510 and -0.462e of NPQC and FQC, respectively. Additionally, the N37 atom of NPQC is also negatively charged and increases the active sites of this inhibitor adsorbed on the metal surface. The presence of more negatively charged centers on NPQC enhances its adsorption and thus its anti-corrosive properties. Alternatively, the TNC values of the common heteroatoms of the protonated forms are smaller than those of the neutral forms. This decreases the interaction between the protonated species and the metal surface. For instance, the TNC of the protonated forms (at O18) of NPQC and FQC in the gas phase are -0.211 and -0.195e, respectively.

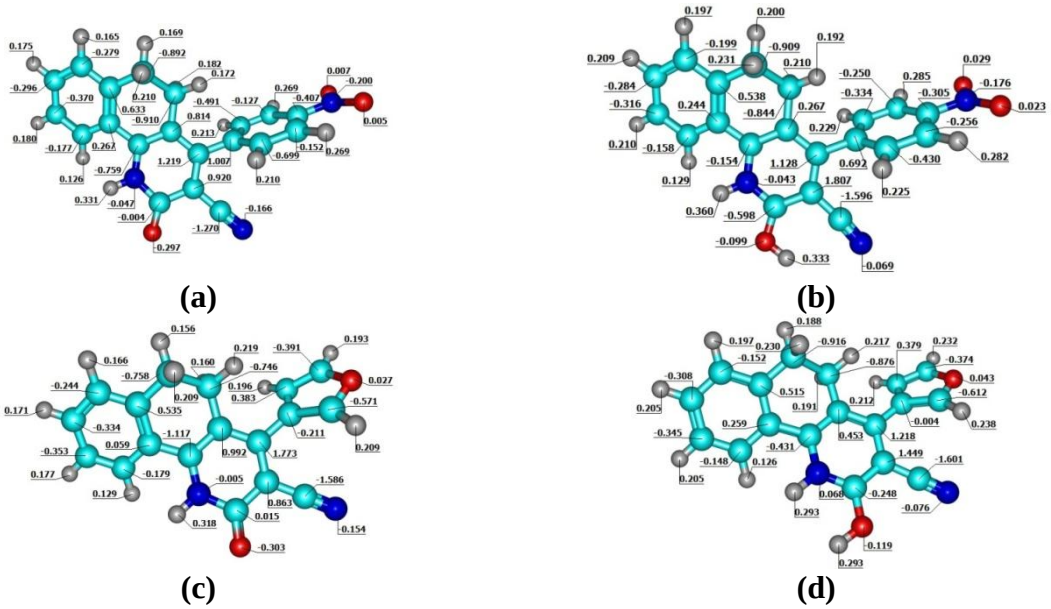

Figure 6. Mulliken charges distribution of the neutral and protonated forms of the investigated inhibitors (a) neutral form of NPQC, (b) protonated form @O18 of NPQC, (c) neutral form of FQC, and (d) protonated form @O18 of FQC at the B3LYP/6-311++G(d,p) in the gas phase.

3.4. Modeling of the neutral and protonated forms of inhibitor-iron complexes

Modeling of the inhibitor-iron (inh–Fe) complexes was aided by the Mulliken population on the heteroatoms and by the molecular electrostatic maps plots of the inhibitor molecules. From the Mulliken charge distribution and molecular electrostatic maps plots, it was possible to recognize the heteroatoms that should be considered. Since only the heteroatoms that are negatively charged are the only ones considered as the active sites for adsorption of the inhibitor molecules on the Fe surface.

The stabilization energy of the complex formed between the iron and the active site of the inhibitor is calculated according to Equation 7: [42, 43]

$$\Delta E_{complex} = E_{inh-Fe} - (E_{inh} + E_{Fe}) \quad \textbf{(7)}$$

where $E_{inh\text{-}Fe}$ is the energy of the complex (inhibitor-Fe) at the different active sites on the inhibitor, E_{inh} is the energy of the monomer inhibitor, and E_{Fe} is the energy of the monomer iron atom. According to Equation 7, as the complex formed becomes more stable, the stabilization energy becomes more negative value and *vice versa*. The optimizations of the inh-Fe complexes for the neutral and protonated forms NPQC and FQC were only successful at the N16 site, which results in complexes with the optimum structures with no imaginary frequencies. Hence, we can say that the N16 site is the preferred site for adsorption on the iron surface. Table 7 shows at the B3LYP/6-31+G(d) level in the gas phase, the complex energies N16 as the active site of the inhibitor molecules, and the N16-Fe bond lengths and the dipole moment values for the NPQC and FQC inhibitors.

Table 7. The complex energy (in kcal/mol) of the (inh-Fe) complexes, N16-Fe bond distance (in Å) and the dipole moments (in Debaye) at the possible active site (N16) of the neutral and protonated forms of NPQC and FQC calculated at the B3LYP/6-31+G(d) in the gas phase.

	Complex (N16-Fe)		
	$\Delta E_{complex}$	bond distance	μ
NPQC	-44.11	1.753	9.70
NPQC (PO18)	-48.45	1.724	11.39
FQC	-43.80	1.758	8.92
FQC (PO18)	-48.10	1.731	5.46

The complex energies are negative values, fallen within a small range, *i.e.* (-43.80)-to-(-48.45 kcal/mol), indicating that the process of complexation resulting in energy minimization, and the larger negative value of complex energy is combined with shorter N16-Fe bond length, thus as the bond becomes shorter it becomes stronger and results in smaller complex energy and thus more stabilization for the complex formed. Another important notice is that the stabilization energies of NPQC-Fe complexes in its neutral and protonated forms are larger than that of FQC-Fe complexes. This may be used to explain the observed better inhibition efficiency of NPQC over FQC. Also, the complexation energies of the inh-Fe complexes with the pronated forms of the two inhibitors are larger than those of the neutral forms. However, as the protonation at O18 site results in decreasing of the reactivity of the two inhibitors (from the calculated QCPs values), it results in stronger adsorption of the inhibitor on the mild steel surface. The weaker adsorption of FQC in its neutral and protonated forms on the Fe surface with respect to that of NPQC could be also justified using the values of dipole moments. Since the dipole moments of the NPQC-Fe complexes are larger than that of FQC-Fe. On the other hand, the dipole moment of neutral form of FQC-Fe is greater than that of the protonated form of this complex and the reverse is true with respect to NPQC inhibitor. Thus, we should consider the properties of inhibitor-Fe complexes as a whole and not only rely on the properties of the isolated inhibitor to assess its performance as anticorrosive.

4. CONCLUSION

The present study combined experimental observations and DFT calculations to investigate the potential of two new derivatives of quinoline-3-carbonitrile (NPQC and FQC) for the protection of steel in a 1.0 M HCl medium. Most of the QCPs correlated very well with the experimental inhibition efficiencies, and confirm on the superiority of NPQC over FQC as an inhibitor. The calculations of all protonation sites revealed that protonation at O18 and N16 for both inhibitors were favored over that at other protonation sites. This was obtained from the MEP plots and calculated proton affinities. From the correlation of the QCPs and experimental inhibition efficiencies, the protonation process decreases the reactivity of the two inhibitors. Conversely, for the two inhibitors, the protonation at O18 site results in larger complexation energies of the inh-Fe complexes than those of the neutral forms.

ACKNOWLEDGEMENTS
Nuha Wazzan gratefully acknowledges King Abdulaziz University's High-Performance Computing Centre (Aziz Supercomputer) (http://hpc.kau.edu.sa) for assisting with the calculations for this paper. The Authors gratefully acknowledge Prof. Hassan Faidallah for providing the NPQC and FQC compounds for the experimental corrosion testing.

References

1. A. Chetouani, B. Hammouti, M. Benkaddour, *Pigment & resin technology*, 33 (2004) 26-31.
2. W.A. Siddique, A. Dubey, *Portugaliae Electrochimica Acta*, 23 (2005) 445-455.
3. E.E. Ebenso, I.B. Obot, L. Murulana, *Int. J. Electrochem. Sci*, 5 (2010) 1574-1586.
4. S. John, A. Joseph, T. Sajini, A.J. Jose, *Egyptian Journal of Petroleum*, (2016).
5. M. Chen, H. Chen, J. Ma, X. Liu, S. Zhang, *Bioorganic & Medicinal Chemistry Letters*, 24 (2014) 2867-2870.
6. N. Nayak, J. Ramprasad, U. Dalimba, *Journal of Fluorine Chemistry*, 183 (2016) 59-68.
7. J. Fiorito, F. Saeed, H. Zhang, A. Staniszewski, Y. Feng, Y.I. Francis, S. Rao, D.M. Thakkar, S.-X. Deng, D.W. Landry, O. Arancio, *European Journal of Medicinal Chemistry*, 60 (2013) 285-294.
8. Y. Hu, N. Green, L.K. Gavrin, K. Janz, N. Kaila, H.-Q. Li, J.R. Thomason, J.W. Cuozzo, J.P. Hall, S. Hsu, C. Nickerson-Nutter, J.-B. Telliez, L.-L. Lin, S. Tam, *Bioorganic & Medicinal Chemistry Letters*, 16 (2006) 6067-6072.
9. Ş. Erdoğan, Z.S. Safi, S. Kaya, D.Ö. Işın, L. Guo, C. Kaya, *Journal of Molecular Structure*, 1134 (2017) 751-761.
10. S.A. Khan, A.M. Asiri, S.H. Al-Thaqafy, H.M. Faidallah, S.A. El-Daly, *Spectrochimica Acta Part A: Molecular and Biomolecular Spectroscopy*, 133 (2014) 141-148.
11. S.S. Abdel-Rehim, K.F. Khaled, N.A. Al-Mobarak, *Arabian Journal of Chemistry*, 4 (2011) 333-337.
12. H. Ma, T. Song, H. Sun, X. Li, *Thin Solid Films*, 516 (2008) 1020-1024.
13. I.B. Obot, Z.M. Gasem, *Corrosion Science*, 83 (2014) 359-366.
14. G.W.T. M. J. Frisch, H. B. Schlegel, G. E. Scuseria, M. A. Robb, J. R. Cheeseman, G. Scalmani, V. Barone, G. A. Petersson, H. Nakatsuji, X. Li, M. Caricato, A. Marenich, J. Bloino, B. G. Janesko, R. Gomperts, B. Mennucci, H. P. Hratchian, J. V. Ortiz, A. F. Izmaylov, J. L. Sonnenberg, D. Williams-Young, F. Ding, F. Lipparini, F. Egidi, J. Goings, B. Peng, A. Petrone, T. Henderson, D. Ranasinghe, V. G. Zakrzewski, J. Gao, N. Rega, G. Zheng, W. Liang, M. Hada, M. Ehara, K. Toyota, R. Fukuda, J. Hasegawa, M. Ishida, T. Nakajima, Y. Honda, O. Kitao, H. Nakai, T. Vreven, K. Throssell, J. A. Montgomery, Jr., J. E. Peralta, F. Ogliaro, M. Bearpark, J. J. Heyd, E. Brothers, K. N. Kudin, V. N. Staroverov, T. Keith, R. Kobayashi, J. Normand, K. Raghavachari, A. Rendell, J. C. Burant, S. S. Iyengar, J. Tomasi, M. Cossi, J. M. Millam, M. Klene, C. Adamo, R. Cammi, J.

W. Ochterski, R. L. Martin, K. Morokuma, O. Farkas, J. B. Foresman, and D. J. Fox, in, Gaussian, Inc., Wallingford CT, 2016.
15. A.D. Becke, *Phys. Rev*. A, 38 (1988) 3098-3100.
16. C. Lee, W. Yang, R.G. Parr, *Physical Review* B, 37 (1988) 785-789.
17. C. Froese Fischer, *Computer Physics Communications*, 43 (1987) 355-365.
18. V. Barone, M. Cossi, *The Journal of Physical Chemistry* A, 102 (1998) 1995-2001.
19. Roy Dennington, T. Keith, J. Millam, in: S. Mission (Ed.), *Semichem Inc*., KS, 2009.
20. G. Zhurko, D. Zhurko, in, 2009.
21. K. Fukui, *Science*, 218 (1982) 747-754.
22. I.B. Obot, D.D. Macdonald, Z.M. Gasem, *Corrosion Science*, 99 (2015) 1-30.
23. F. Bentiss, M. Traisnel, H. Vezin, H.F. Hildebrand, M. Lagrenée, *Corrosion Science*, 46 (2004) 2781-2792.
24. I.B. Obot, N.O. Obi-Egbedi, *Corrosion Science*, 52 (2010) 657-660.
25. N.A. Wazzan, *J. Ind. Eng. Chem.*, 26 (2015) 291-308.
26. D.-q. Zhang, Z.-x. An, Q.-y. Pan, L.-x. Gao, G.-d. Zhou, Corrosion Science, 48 (2006) 1437-1448.
27. G. Gao, C. Liang, *Electrochimica Acta*, 52 (2007) 4554-4559.
28. Y.-M. Tang, W.-Z. Yang, X.-S. Yin, Y. Liu, R. Wan, J.-T. Wang, *Materials Chemistry and Physics*, 116 (2009) 479-483.
29. R.G. Parr, R.G. Pearson, *J. Am. Chem. Soc.*, 105 (1983) 7512.
30. J.F. Janak, *Physical Review* B, 18 (1978) 7165-7168.
31. L. Von Szentpály, *Journal of Molecular Structure*: THEOCHEM, 233 (1991) 71-81.
32. R.G. Pearson, *Coordination Chemistry Reviews*, 100 (1990) 403-425.
33. R.G. Pearson, *Inorganic Chemistry*, 27 (1988) 734-740.
34. B. El Ibrahimi, A. Soumoue, A. Jmiai, H. Bourzi, R. Oukhrib, K. El Mouaden, S. El Issami, L. Bazzi, *Journal of Molecular Structure*, 1125 (2016) 93-102.
35. R.G. Parr, L.s.v. SzentpÃ¡ly, S. Liu, *J. Am. Chem. Soc.*, 121 (1999) 1922-1924.
36. N.O. Obi-Egbedi, I.B. Obot, M.I. El-Khaiary, *J. Mol. Struct.*, 1002 (2011) 86-96.
37. V.S. Sastri, J.R. Perumareddi, *CORROSION*, 53 (1997) 617-622.
38. I. Lukovits, E. Kalman, F. Zucchi, *Corrosion*, 57 (2001) 3-8.
39. B. Gomez, N.V. Likhanova, M.A. Dominguez-Aguilar, R. Martinez-Palou, A. Vela, J.L. Gasquez, *The Journal of Physical Chemistry* B, 110 (2006) 8928-8934.
40. E.E. Ebenso, T. Arslan, F. Kandemirlı, I. Love, C.l. Öğretır, M. Saracoğlu, S.A. Umoren, *Int. J. Quantum Chem.*, 110 (2009) 2614-2636.
41. M.K. Awad, M.R. Mustafa, M.M.A. Elnga, *Journal of Molecular Structure: THEOCHEM*, 959 (2010) 66-74.
42. E.E. Ebenso, M.M. Kabanda, T. Arslan, M. Saracoglu, F. Kandemirli, L.C. Murulana, A.K. Singh, S.K. Shukla, B. Hammouti, K.F. Khaled, M.A. Quraishi, I.B. Obot, N.O. Eddy, *Int. J. Electrochem. Sci.* , 7 (2012) 5643-5676.
43. N.O. Eddy, H. Momoh-Yahaya, E.E. Oguzie, *Journal of Advanced Research*, 6 (2015) 203-217.